

# Deterministic Self-Rolling of Ultrathin Nanocrystalline Diamond Nanomembranes for 3D Tubular/Helical Architecture

Ziao Tian, Lina Zhang, Yangfu Fang, Borui Xu, Shiwei Tang, Nan Hu, Zhenghua An, Zi Chen,\* and Yongfeng Mei\*

3D mesostructures assembled<sup>[1–3]</sup> and self-assembled<sup>[4–7]</sup> with organic and inorganic nanomembrane materials have enabled many applications.<sup>[1–13]</sup> A reduction in flexural rigidity allows inorganic nanomembranes less than a few hundred nanometers thick to form complex 3D geometries,<sup>[1,6]</sup> such as tubes,<sup>[14]</sup> helices,<sup>[15–18]</sup> boxes,<sup>[19]</sup> and pop-up buckles.<sup>[20]</sup> Diamond has been constructed into micro- and nanoscale rings,<sup>[21,22]</sup> beams,<sup>[23,24]</sup> and cantilevers,<sup>[25]</sup> for applications in micro- and nanoelectromechanical system,<sup>[26]</sup> microcavities,<sup>[22]</sup> plastic electronics,<sup>[27]</sup> and quantum optics.<sup>[28]</sup> Recently, efforts have been focused on freestanding diamond ribbons and membranes,<sup>[29–33]</sup> which can be fabricated through top-down manufacture methods such as ion slicing,<sup>[31,34]</sup> galvanic etching,<sup>[29]</sup> angle etching,<sup>[35]</sup> and ion beam milling.<sup>[36,37]</sup> However, it is still challenging to assemble and self-assemble diamond membranes into 3D architectures at the micro- and nanoscale due to its extreme hardness.<sup>[27]</sup>

Rolled-up nanotechnology,<sup>[14,38]</sup> as one of the self-assemble methods combined with top-down approach, has attracted great interest and continuous effort for potential applications, e.g., lab-in-a-tube,<sup>[39]</sup> on-chip energy storage,<sup>[40]</sup> optical microcavity,<sup>[41]</sup> and micro/nanomotor.<sup>[42]</sup> In this work, by thinning nanocrystalline (NC) diamond membranes, we reduce their flexural rigidities and roll them into 3D structures (including tubes, jagged ribbons, nested tubes, nested rings, and helices)

from predefined patterns. The diameter of the tube can range from several micrometers to several tens of micrometers by changing the thickness and built-in strain of the diamond nanomembranes. NC-diamond “hockey-stick”-shaped stripes can release from a substrate and transition into helical microscale architectures through controlled debonding.

This process can be simulated using transient quasistatic finite-element methods (FEM) and demonstrates a versatile method to construct helical microstructures from mechanically isotropic NC-diamond membranes. Rolled-up NC-diamond tubular microcavities, with a pronounced nitrogen-vacancy (NV) center-related photoluminescence emission, present optical whisper gallery mode resonance with high quality factors (*Q*-factors) of up to  $10^3$ . Our work provides a new platform to engineer and assemble diamond nanomembranes into 3D mesostructures for potential applications in mechanics,<sup>[25]</sup> photonics,<sup>[35]</sup> and electronics.<sup>[27]</sup>

Bulk diamonds as shown in **Figure 1a-I** have carbon atoms arranged through tetrahedral  $sp^3$  hybridization, giving the highest known atomic density, which provides diamond with superior mechanical properties such as the highest Young's modulus, hardness, and a very low Poisson's ratio. For NC diamond, the most obvious deviations from natural diamond are the grain boundaries. While forming the boundary between crystallites with different orientations, they consist largely of disordered carbon bonded by  $\sigma$  bonds. However, as long as the bulk properties remain dominated by the grains and not the grain boundaries, nanocrystals can be a technologically excellent product showing similar properties to that of bulk single crystals.<sup>[43]</sup> In our experiments, NC-diamond thin films on thermal oxidized silicon substrates are deposited by chemical vapor deposition (CVD) and are provided by Advanced Diamond Technologies (ADT), Inc. By selectively removing silicon oxide, NC-diamond thin films with a thickness of 40 nm release from the substrate and become freestanding nanomembranes as shown in **Figure 1a-II**. Since the bending rigidity of a thin plate scales with the cube of its thickness, the thinner an NC-diamond nanomembrane gets the lower its bending rigidity becomes to facilitate bending or rolling. After NC-diamond nanomembranes are released from the substrates to become freestanding, they can curve or fold out of the plane and form scrolls downward as shown in **Figure 1a-III**. Their detailed microstructures are characterized by transmission electron microscopy (TEM) as shown in **Figure 1a-IV**, and corresponding selected area electron diffraction pattern (the upper image in **Figure 1a-V**) and high-resolution TEM image (the

Z. A. Tian, Y. F. Fang, B. R. Xu,  
Dr. S. W. Tang, Prof. Y. F. Mei  
Department of Materials Science  
Fudan University  
200433 Shanghai, P. R. China  
E-mail: yfm@fudan.edu.cn

Z. A. Tian, Prof. Z. H. An  
State Key Laboratory of Surface Physics  
Key Laboratory of Micro and Nano Photonic Structures  
(Ministry of Education) and Institute of Advanced Materials  
Fudan University  
200433 Shanghai, P. R. China

Dr. L. N. Zhang, Dr. N. Hu, Prof. Z. Chen  
Thayer School of Engineering  
Dartmouth College  
Hanover, 03755 NH, USA  
E-mail: zi.chen@dartmouth.edu

Dr. L. N. Zhang  
Department of Engineering Mechanics  
Shanghai Jiao Tong University  
Dongchuan Rd 800, 200240 Shanghai, P. R. China

DOI: 10.1002/adma.201604572



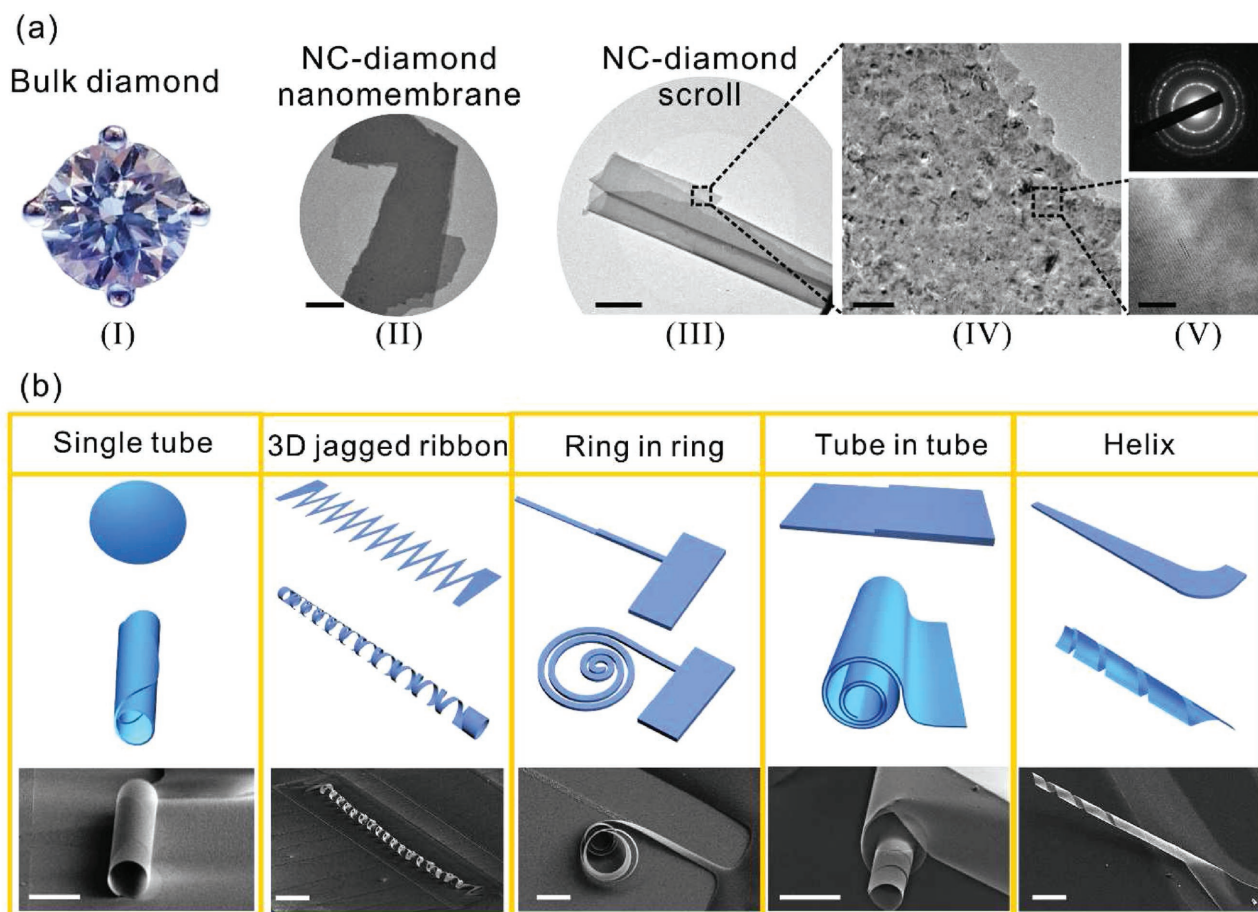


**Figure 1.** Diamond nanomembrane characterization. a) Self-rolling geometries. Scale bars: II) 10  $\mu\text{m}$ , III) 5  $\mu\text{m}$ , IV) 100 nm, and V) 2 nm. I) Optical image of bulk diamonds. II) SEM image of NC-diamond nanomembrane. III) SEM image of an NC-diamond microtube. IV) Enlarged TEM image of the diamond tube wall. V, upper) Selected area electron diffraction pattern of NC-diamond nanomembrane. V, lower) High-resolution TEM image of NC-diamond nanomembrane. b) 2D patterns, 3D predictions, and SEM images for five 3D mesostructures of NC-diamond nanomembranes. Scale bars: 10  $\mu\text{m}$ .

lower image in Figure 1a-V) reveal ultra-nanocrystalline diamonds in our nanomembranes.

Since the rolled-up process is compatible with conventional photolithography processing, curved structures could be constructed with predefined patterns.<sup>[16]</sup> For example, a single tube was rolled up from a prepatterned NC-diamond nanomembrane through an under-etching process shown in upper part (I–III) of Figure S1 (see details in the Supporting Information). A 500 nm thick silicon oxide film is deposited onto the photolithography-patterned samples as a reactive ion etching (RIE) template. A predefined NC-diamond nanomembrane is formed with RIE process that allows it to be undercut and released. Upon immersion into hydrofluoric acid solution, the nanomembrane was detached from the substrate and self-rolled up into a single tube driven by its intrinsic stress gradient. In Figure 1b, the first column shows a rolled-up NC-diamond tube formed from a circular pattern and the second column a rolled-up 3D mesostructure from a jagged ribbon pattern. In contrast to the thickness modulation of a defined nanomembrane by deposition,<sup>[44]</sup> we employed an RIE-thinning method to regulate the thickness of NC-diamond nanomembranes as shown in the lower part (IV–VI) of Figure S1 (see details in the Supporting

Information) for the fabrication of mesostructures, e.g., nested tube (i.e., tube in tube) and nested ring (i.e., ring in ring). A thickness-modulated NC-diamond ribbon is self-rolled up into the ring-in-ring structure (third column in Figure 1b) whereas a thickness-modulated squared nanomembrane is formed into the tube in tube structure (forth column). Interestingly, unlike circular or squared nanomembranes, a “hockey-stick”-shaped nanomembrane is geometrically asymmetric and curls into helical structures spontaneously in order to reduce elastic energy, which provides a new opportunity for precise control of the helical shape formation and will be discussed in the following text.

It is known that there are two basic parameters that control the diameter of rolled-up tubes: strain gradient and layer thickness.<sup>[16]</sup> Both parameters can be employed during the layer growth and post-fabrication. In our NC-diamond nanomembranes, the rolling is always downward as shown in Figure S2a,b (Supporting Information). With the assistance of Raman scattering measurement (Figure S2c, Supporting Information), it is found that NC-diamond films on substrate present tensile strain on average. Meanwhile, it is noted that NC-diamond films reveal tensile or compressive strains depending on the deposition conditions.<sup>[45,46]</sup> Hence, it can be inferred

that NC nanomembranes before rolling present the strain gradient as follows: larger tensile strain close to the interface between films and substrates and smaller tensile strain close to the surface, which is consistent with the previous report<sup>[45]</sup> and our Raman measurement (see details in the Supporting Information). Hence, we can refer to the former layer as the strain layer and latter one as the relax layer. In another way, the layer thickness can fine tune the tube diameter based on the classical Timoshenko formula.<sup>[47,48]</sup> To simplify the calculation of the diameter but still to obtain accurate values,<sup>[48]</sup> we apply the following equation in our rolled-up NC-diamond nanomembranes:

$$D = \frac{(t_{\text{strain}} + t_{\text{relax}}) \left[ 3(1+m)^2 + (1+m) \left( m^2 + \frac{1}{m} \right) \right]}{3\Delta\varepsilon(1+\nu)(1+m)^2} \quad (1)$$

where  $t_{\text{strain}}$  and  $t_{\text{relax}}$  are the respective thicknesses of the tensile and relaxed strain layers,  $m = t_{\text{strain}}/t_{\text{relax}}$  is their ratio,  $\Delta\varepsilon$  is the strain difference between two layers,  $\nu$  is the Poisson's ratio, and  $D$  is the tube diameter. In our experiments, the RIE thinning is adopted to control the nanomembrane thickness, thereby tuning the tube diameter. As shown in Figure 2a, the diameter of rolled-up NC-diamond microtubes is proportional

to the nanomembrane thickness (black spheres), and their scanning electron microscopy (SEM) images are exhibited as insets. An array of rolled-up NC-diamond microtubes formed on circular etching patterns are exhibited in Figure 2b (optical microscope image). The microtubes, about 50  $\mu\text{m}$  in diameter and 500  $\mu\text{m}$  in length, are well arranged in a highly ordered manner and aligned in the same direction. Based on Equation (1), the blue line in Figure 2a shows the calculated curve and reveals an obvious variation in comparison with our experimental data. The experimental diameter is smaller than the theoretical values. Therefore, there could be an unexpected effect in the rolled-up NC-diamond nanomembranes. By using atomic force microscopy (AFM), we carefully investigated the surface morphology of NC-diamond nanomembranes before (Figure 2c) and after (Figure 2d) etching with RIE in oxygen plasma. Before etching, NC-diamond films grown on the substrate exhibit a smooth and uniform surface. However, their rough surface was observed after etching with RIE, which suggests that the effective thickness contributing to rolling could be thinner than the AFM-measured thickness as schematically shown in Figure 2e. Hence, the thickness of the relax layer is reduced from the nominal one ( $t$ ) to the effective one ( $t_{\text{eff}}$ ) and thus assisting the rolling as sketched in Figure 2f. When  $t_{\text{eff}}$  is used instead of  $t$ , the red line in Figure 2a shows the

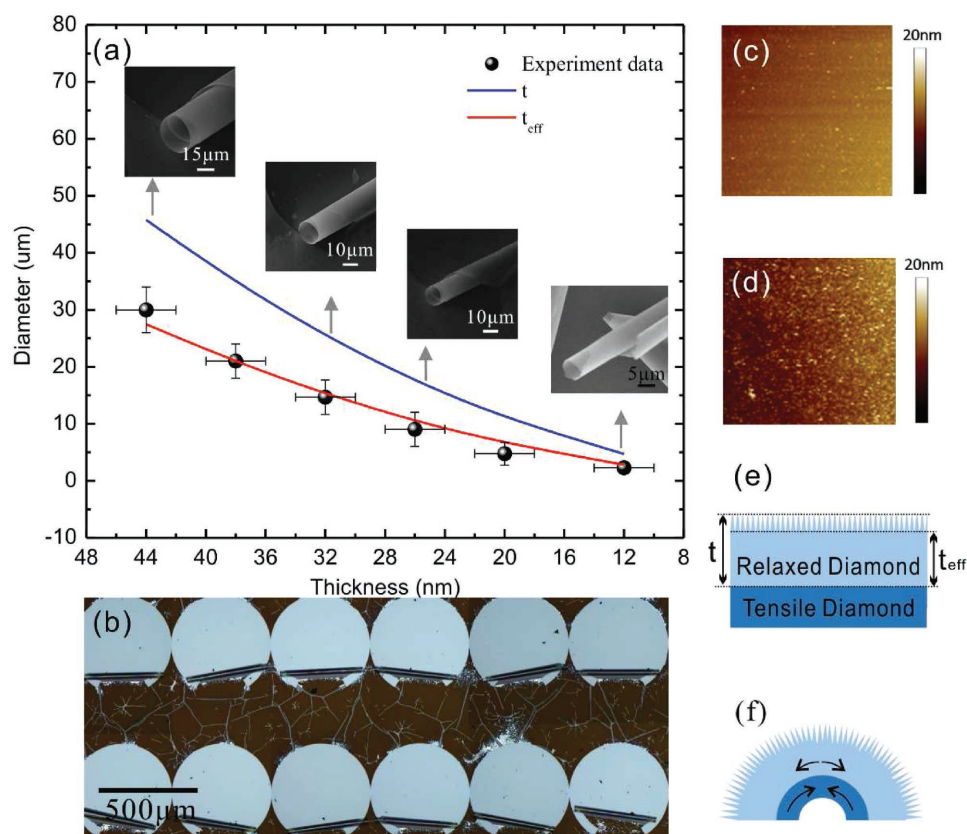


**Figure 2.** Diamond nanomembranes thinning and rolling control. a) Diameter of a single tube as a function of the diamond nanomembranes thickness after RIE etching. Insets show corresponding SEM images of microtubes with various diameters. b) Optical microscope image of ordered microtube arrays from NC diamond. c,d) The surface morphology of diamond films before and after etching with RIE in oxygen plasma by AFM imaging (1  $\mu\text{m} \times 1 \mu\text{m}$ ). e,f) Schematic of an inverted rolling up process relevant for partially strain-relaxed films. A region with thickness  $t_{\text{eff}}$  and  $t$  represents the region of effective thickness and nominal thickness. The arrows represent the contraction and expansion.

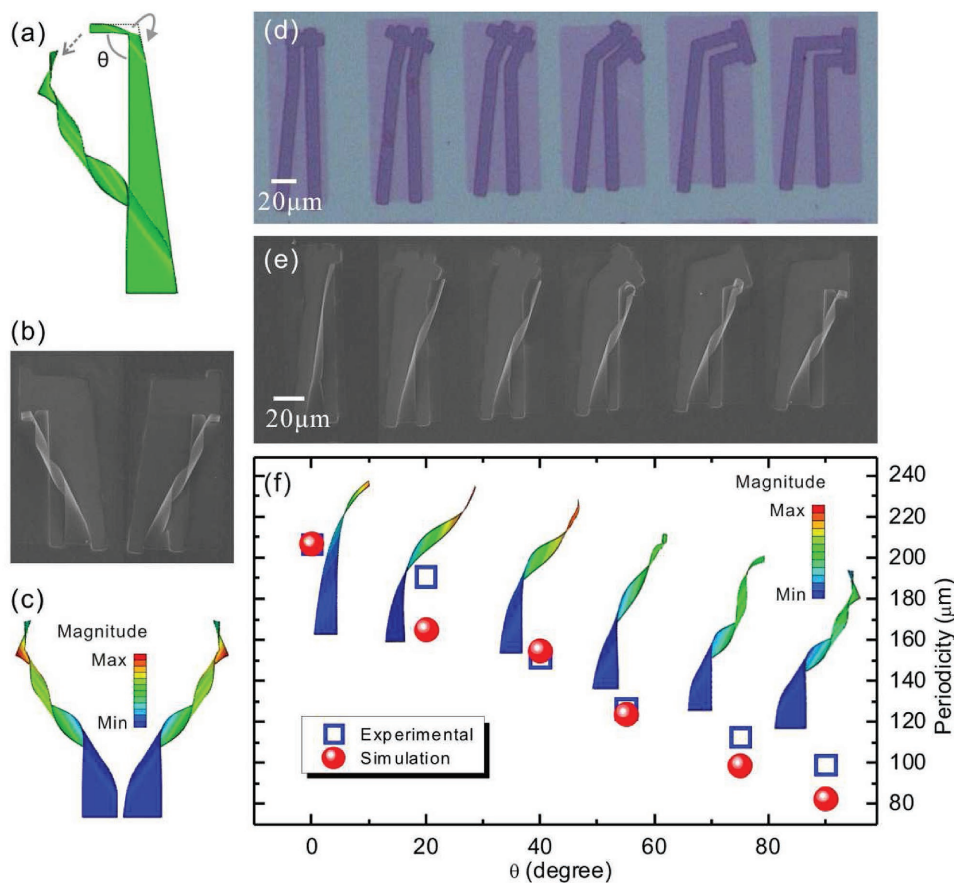


**Figure 3.** Directional rolling of isotropic diamond nanomembranes. a) Schematic drawing illustrating a 2D “hockey stick” shape with inclined angle  $\theta$ . b) SEM images of helix with inverted chirality. c) Result of FEM simulation. d,e) Optical images of 2D shapes with different inclined angle  $\theta$  (d) and SEM images of diamond helices with different inclined angle  $\theta$  (e). The sample from left to right have inclined angle  $\theta = 90^\circ, 75^\circ, 55^\circ, 40^\circ, 20^\circ$ , and  $0^\circ$ , respectively. f) Comparison of simulation and experiment for periodicity at various inclined angles  $\theta$ . Insets show the displacement contour plot of the FEM of the “hockey stick” shapes at various inclined angles  $\theta$ .

calculated values from Equation (1), which can agree well with our experimental data with the fitting parameters,  $\Delta\varepsilon = 0.7\%$  and  $t_{\text{strain}} = 2.0$  nm which is equal to the critical thickness of NC-diamond films with a tensile strain (see details in the Supporting Information).

Directional rolling can be controlled by anisotropic mechanical property<sup>[15]</sup> and geometry design<sup>[49]</sup> of pre-rolling nanomembranes. The latter one can be applied in isotropic materials for long-side directional rolling due to the minimization of the total elastic energy in a rectangular-shaped nanomembranes<sup>[49]</sup> which is still challenging to achieve, although the corner effect has been proposed to guide bilayer bending.<sup>[50]</sup> In this study, we found that a series of helical structures can be formed in our NC-diamond nanomembranes with isotropic mechanical properties when the asymmetric geometry is carefully designed. As sketched in Figure 3a, we defined a nanomembrane strip like “hockey stick” with the inclined angle  $\theta$ . Such strip can roll from a corner (curved arrow) and form a helical structure. Experimentally, such rolling can be controlled by rolling chirality as shown in Figure 3b, which well agrees with the simulation results (Figure 3c). Although there was observation of short-side rolling in a rectangular nanomembrane previously,<sup>[49,50]</sup> directional rolling for helical structure is

seldom reported on nanomembranes with isotropic mechanical properties. The rolling behavior here also defers from the rolling of helical ribbons with isotropic mechanical properties but subjected to anisotropic driving forces.<sup>[51,52]</sup>

From the energetic perspective, a nanomembrane always starts rolling from the long side to minimize the total elastic energy, however, short-side rolling has been observed experimentally, which could be attributed to a history-dependent process.<sup>[49]</sup> During the etching process, an NC-diamond nanomembrane with a “hockey stick” shape was cut off from the head part and subsequently released from the head to the knob parts. Such a release process is due to the narrower width in the head part as compared with that in the knob part with the same etching rate. We simulated such release process as shown in Figure S5 (Supporting Information) with the minimization of the total elastic energy, where the corner area (marked by the curved arrow in Figure 3a) started to roll if we only released the head part until  $9\ \mu\text{m}$  (from head to knob). The first release area is determined by the etching rate and the nanomembrane geometry. Such corner-dominated rolling keeps going when the release continues and thus enables a helical structure as shown Figure S6 (Supporting Information), which reveals a whole rolling process with a moving boundary

condition. This procedure agrees well with our etching process due to our designed special shape—“hockey stick”—and the principle revealed in this study can be further used to design other geometric shapes to control the rolling process with history-dependent effect. To showcase the feasibility with a simple example, we adjusted the inclined angle  $\theta$  to control the helical periodicity as shown in Figure 3d–f. Prepatterned NC-diamond nanomembranes are designed to have various angles,  $0^\circ$ ,  $20^\circ$ ,  $40^\circ$ ,  $55^\circ$ ,  $75^\circ$ , and  $90^\circ$ . Their corresponding optical microscope images are shown from left to right in Figure 3d, while the rolled-up helices are formed after releasing from the substrate as shown in Figure 3e (SEM images). The inclined angle can well control the helical periodicities of our designed NC-diamond stripes. In Figure 3f, we summarize the experimental data and compare it with the simulation results on helical periodicities. Detailed simulation analysis can be found in the Supporting Information. In most cases, simulation results agree well with the experimental data, while there is some notable discrepancy when the inclined angle is  $20^\circ$ . This discrepancy may be due to the limitation of photolithography and RIE resolution, which could lead to the mismatch of patterns between the experiment and simulation. It is also worth mentioning that the dimensions of the nanomembrane fall into the wider regime where the structure would have been multistable if the shape had some symmetry (e.g., being circular or square).<sup>[52]</sup> The calculated value of the dimensionless parameter for multistability is  $\eta = W\sqrt{\kappa/H} \geq 2.5$ , larger than the critical value  $\eta = \sqrt[3]{80(1+\nu)}/3 = 2.3$ , where  $W$  and  $H$  are the respective width and thickness of stick,  $\nu$  is the Poisson's ratio, and  $\kappa$  is the curvature.<sup>[53,54]</sup> However, due to the geometric asymmetry and the release (or debonding) history, the result configuration is deterministic.

Befitting from the unique optical properties of NV centers,<sup>[55]</sup> a number of studies on diamond have been focused on the color center-cavity coupling by using a diamond resonator or a separate optical resonator to defect centers.<sup>[21–25,28]</sup> With the rolled-up method, tubular optical microcavities can be constructed from defined flat nanomembranes, which can offer large flexibility from fabrication to applications.<sup>[6]</sup> Hence, NC-diamond nanomembranes can be self-rolled up as tubular microcavities as presented in Figure 4. Starting from an NC-diamond planar film with a circular diameter of  $100\ \mu\text{m}$  and around  $25\ \text{nm}$  in thickness, an NC-diamond microcavity is formed with rolled-up tube diameters of  $12\ \mu\text{m}$  (upper),  $16\ \mu\text{m}$  (middle), and  $20\ \mu\text{m}$  (down), which are shown in Figure 4a. Their corresponding nanomembrane thicknesses are around  $22$ ,  $26$ , and  $29\ \text{nm}$ . Photoluminescence (PL) spectra of a planar film (black line) and a rolled-up tube with a diameter of  $20\ \mu\text{m}$  (red line) were excited by a  $532\ \text{nm}$  laser line using micro-PL setup (the other two PL spectra are shown in Figure S7 in the Supporting Information). As presented in Figure 4b, there are three PL emissions: i) a broad emission band from the defect states among NC grains<sup>[47]</sup> which can cover the whole spectra range, ii) a peak from  $\text{NV}^-$  centers (marked arrows) located at  $637\ \text{nm}$ , and iii) Raman signals (marked by dashed line) at  $574$  and  $580\ \text{nm}$  originated from graphite and diamond-like bonds.<sup>[47]</sup> In the case of a rolled-up tube, the PL spectrum (red line in Figure 4b) shows an obvious intensity modulation due to PL light coupled to the whisper gallery modes of the

microtube with a  $Q$ -factor of more than one thousand. Comparing to planar films, the spontaneous PL emission of NVs is dramatically enhanced by one order of magnitude, which can be attributed to the light-trapping effect in the tubular geometry. Interestingly, such rolled-up tubular optical microcavity presents stable PL resonance modes when the laser excitation power increases as shown in the inset of Figure 4b. The laser spot size on the sample was  $1.5\ \mu\text{m}$  in diameter and the laser power was from  $2.5$  to  $25\ \text{mW}$ . The resonance peak position (PP) at  $641.0\ \text{nm}$  (mode #196 marked by the dark triangle in Figure 4b) has almost no shift (see details in Section 5 of the Supporting Information). It is known that the tube presents a poor thermal conductivity because of its hollow structure.<sup>[56]</sup> However, our NC-diamond microtubes are stable even under the maximal excitation power ( $25\ \text{mW}$ ) of our PL setup since diamond has the high thermal conductivity ( $2000\ \text{W m}^{-1}\ \text{K}^{-1}$ ) and low thermo-optic coefficient of  $(dn/dT) = 10 \times 10^{-6}\ \text{K}^{-1}$ .<sup>[22]</sup>

The nanomembrane thickness can change the diameter of rolled-up microtubes as discussed before, while it can also tune their resonance properties, such as resonance peak position and  $Q$ -factors.<sup>[57]</sup> As shown in Figure 4c, we adopted rolled-up tubes with diameters larger than  $10\ \mu\text{m}$  and the nanomembrane thickness of larger than  $20\ \text{nm}$ <sup>[58]</sup> because there would be a critical wall thickness for resonance modes, which can confine the light inside.<sup>[59]</sup> With the increase of nanomembrane thicknesses, the  $Q$ -factors are enhanced due to the improved confinement of light. Such confinement can also be influenced by the tube diameter, which suggests that a tube with a larger radius can induce a better light propagation in the tube wall with less bending. Hence, it remains a challenge to get a strong light resonance in the rolled-up NC-diamond tube with a diameter smaller than  $10\ \mu\text{m}$ . The polarization state of the resonance modes was checked with our NC-diamond tubular microcavities as shown in Figure 4d. On the NC-diamond tube with a diameter of  $20\ \mu\text{m}$ , we measured the transverse-magnetic mode polarization by recording PL spectra after a rotating lambda half wave plate and a fixed linear polarizer positioned in front of our spectrometer. In Figure 4b, the average peak-to-valley ratio for the mode 196 (marked by the dark triangle in Figure 4b) is exhibited as a function of the rotating angle between the tube axis and the polarizer axis. This data shows that the optical resonant modes observed in the PL spectra are strictly polarized along the tube axis, which is caused by the total reflection of the light at the tube walls. Therefore, rolled-up microtubes could be a general platform for optical cavities to generate the polarized resonance emission through materials integration (for example, diamond here) and geometry design.<sup>[59]</sup>

In conclusion, we have rolled up nanocrystalline diamond nanomembranes into a variety of 3D architectures, including a single tube, 3D jagged ribbon, helix, tube in tube, and ring in ring by selective etching. The flexural rigidities of NC-diamond nanomembranes are greatly reduced by thinning the thickness, and thus enabling large deformation like rolling or bending with a wide range of curvatures. Interestingly, strong evidence of pathway-determined rolling is found in helical structures, which are released from selectively designed patterns of NC-diamond nanomembranes, and the mechanical principle is unveiled through a combination of experiments and

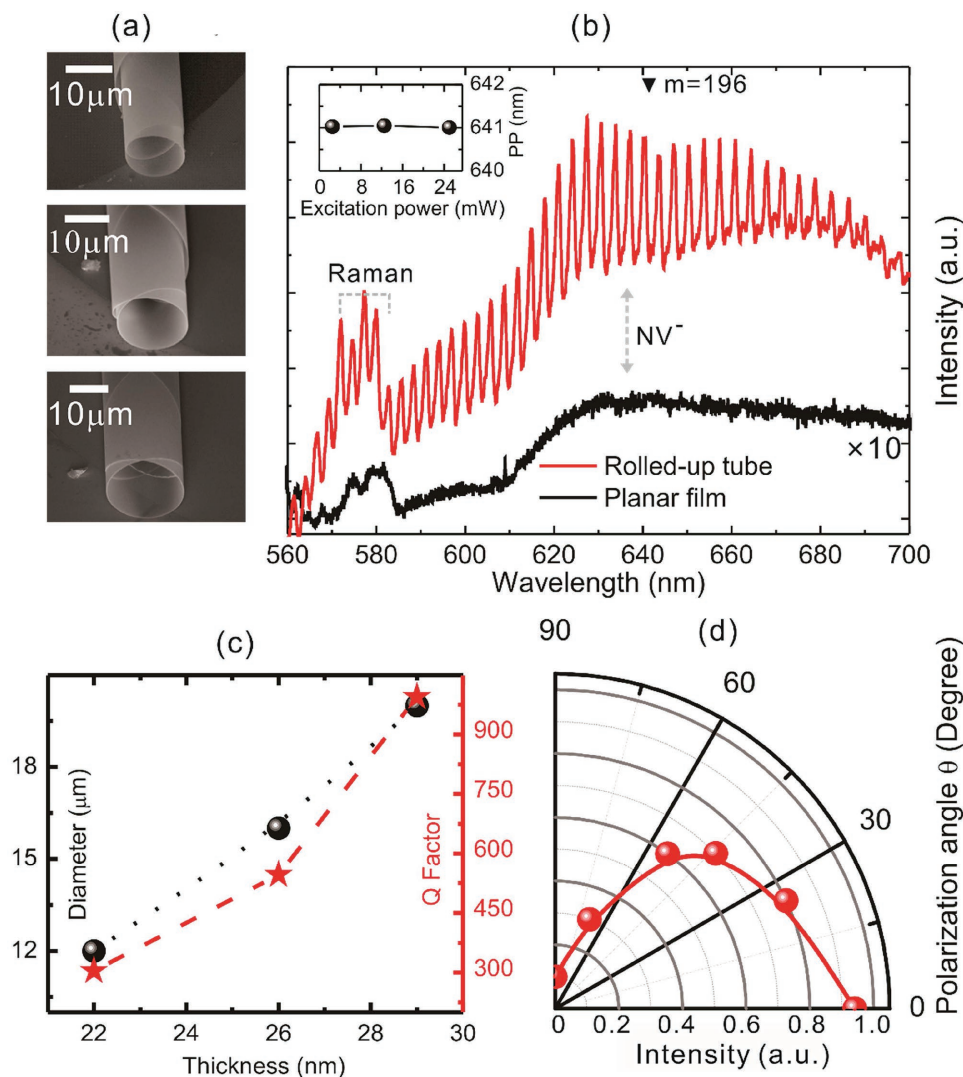


**Figure 4.** Optical characterization of diamond microtubes. a) SEM image of diamond microtube with diameter of 12  $\mu\text{m}$  (upper), 16  $\mu\text{m}$  (middle), and 20  $\mu\text{m}$  (down), respectively. b) PL spectra of a planar film (black line) and a rolled-up tube (red line). Inset shows a dependence of a resonance peak position (PP) (mode number = 196) on excitation power. c) Thickness effect on coupling strength between NVs and tubular diamond resonator. Red line showing the relationship between  $Q$ -factor and thickness of tube. Black line showing the relationship between diameter of tube and thickness of tube. d) PL measurement of diamond microtube at room temperature for different polarization configurations.

finite-element simulations. Moreover, rolled-up NC-diamond tubular microcavities present strong and stable optical resonance and reveal polarization-dependent light emission, which is related to  $\text{NV}^-$  centers. The findings imply that such a rolled-up process can be applied to most of inorganic hard materials including diamond and could suggest significant potential in self-assembly and assembly of diamond nanomembranes or other rigid nanomembranes.

## Experimental Section

**Nanocrystalline Diamond Film Wafer:** NC diamond (known as Aqua 25 from Advanced Diamond Technologies (ADT), Inc.) was grown using the hot-filament-assisted CVD technique at 680  $^{\circ}\text{C}$  on silicon wafers (diameter = 150 mm) using a predominantly methane/hydrogen growth

chemistry. The average film thickness was measured as around 40 nm with a uniformity of within 11% across the wafer with the thickness greatest at the center.

**Fabrication of Rolled-Up Diamond Microtubes:** Nanocrystalline diamond films on substrates were patterned by photolithography and RIE. First, spin casting and photolithography defined patterns of photoresist using AZ-5214 (Microchemicals GmbH, Germany) with about 1  $\mu\text{m}$  in thickness. Second, the patterned film was etched using RIE under the following conditions: oxygen gas flow rate 50 standard cubic centimeters per minute, chamber pressure 15 mT, and bias at 200 V. After that, a 40% HF (hydrofluoric acid) solution was used to selectively remove the  $\text{SiO}_2$  layer to undercut and release the film as the nanomembrane. The etching rate is around 60  $\text{nm min}^{-1}$ . Finally, critical point drying (CPD030 Critical Point Dryer from Bal-Tec AG) was applied to dry the rolled-up nanomembranes without structural collapse.

**Finite-Element Analysis:** The simulation applies linear elastic mechanics to analyze the release of 3D “hockey-stick”-shaped nanomembranes under an initial biaxial strain. The elastic modulus and

Poisson's ratio for nanocrystalline diamond nanomembranes are 980 GPa and 0.069, respectively. The substrate boundary was rigidly fixed, and the side boundary was free to move in plane. To simulate initial etching process, only the head of the "hockey stick" was selectively released by applying the appropriate boundary conditions.

**Microtube-Based Optical Resonators:** A 532 nm laser line acted as the excitation light for both micro-photoluminescence ( $\mu$ -PL) and micro-Raman spectra, while 325 nm laser line was only adopted for micro-Raman measurement. The excitation laser was focused through microscope objectives and the emission signal from nanocrystalline diamond was collected through the same objective to record the spectra.

## Supporting Information

Supporting Information is available from the Wiley Online Library or from the author.

## Acknowledgements

This work was supported by the Natural Science Foundation of China (Grant Nos. 51322201 and U1632115) and Science and Technology Commission of Shanghai Municipality (Grant No. 14JC1400200). Z.C. acknowledges the support from the Society in Science–Branco Weiss fellowship, administered by ETH Zürich. The authors thank Ian Trase for language improvement. Part of the experimental work was carried out in the Fudan Nanofabrication Laboratory.

Received: August 26, 2016

Revised: November 21, 2016

Published online: February 6, 2017

- [1] J. A. Rogers, M. G. Lagally, R. G. Nuzzo, *Nature* **2011**, *477*, 45.
- [2] S. Xu, Z. Yan, K.-I. Jang, W. Huang, H. Fu, J. Kim, Z. Wei, M. Flavin, J. McCracken, R. Wang, A. Badea, Y. Liu, D. Xiao, G. Zhou, J. Lee, H. U. Chung, H. Cheng, W. Ren, A. Banks, X. Li, U. Paik, R. G. Nuzzo, Y. Huang, Y. Zhang, J. A. Rogers, *Science* **2015**, *347*, 149.
- [3] C. Xie, J. Liu, T. M. Fu, X. Dai, W. Zhou, C. M. Lieber, *Nat. Mater.* **2015**, *14*, 1286.
- [4] F. Cavallo, M. G. Lagally, *Soft Matter* **2010**, *6*, 439.
- [5] V. B. Shenoy, D. H. Gracias, *MRS Bull.* **2012**, *37*, 847.
- [6] G. Huang, Y. Mei, *Adv. Mater.* **2012**, *24*, 2517.
- [7] C. Ye, V. V. Tsukruk, *Science* **2015**, *347*, 130.
- [8] W. Huang, X. Yu, P. Froeter, R. Xu, P. Ferreira, X. Li, *Nano Lett.* **2012**, *12*, 6283.
- [9] G. Huang, Y. Mei, D. J. Thurmer, E. Coric, O. G. Schmidt, *Lab Chip* **2009**, *9*, 263.
- [10] D. Karnaushenko, D. D. Karnaushenko, D. Makarov, S. Baunack, R. Schäfer, O. G. Schmidt, *Adv. Mater.* **2015**, *27*, 6582.
- [11] R. Sharma, C. C. B. Bufon, D. Grimm, R. Sommer, A. Wollatz, J. Schadowald, D. J. Thurmer, P. F. Siles, M. Bauer, O. G. Schmidt, *Adv. Energy Mater.* **2014**, *4*, 1301631.
- [12] L. Ionov, *Polym. Rev.* **2013**, *53*, 92.
- [13] X. Yu, W. Huang, M. Li, T. M. Comberiate, S. Gong, J. E. Schutt-Aine, X. Li, *Sci. Rep.* **2015**, *5*, 9661.
- [14] O. G. Schmidt, K. Eberl, *Nature* **2001**, *410*, 168.
- [15] D. J. Bell, L. Dong, B. J. Nelson, M. Golling, L. Zhang, D. Grützmacher, *Nano Lett.* **2006**, *6*, 725.
- [16] P. Froeter, X. Yu, W. Huang, F. Du, M. Li, I. Chun, S. H. Kim, K. J. Hsia, J. A. Rogers, X. Li, *Nanotechnology* **2013**, *24*, 475301.
- [17] Z. Chen, *Nanoscale* **2014**, *6*, 9443.
- [18] Z. Chen, G. S. Huang, I. Trase, X. M. Han, Y. Mei, *Phys. Rev. Appl.* **2016**, *5*, 017001.
- [19] J. Cho, D. H. Gracias, *Nano Lett.* **2009**, *9*, 4049.
- [20] Y. Zhang, Z. Yan, K. Nan, D. Xiao, Y. Liu, H. Luan, H. Fu, X. Wang, Q. Yang, J. Wang, W. Ren, H. Si, F. Liu, L. Yang, H. Li, J. Wang, X. Guo, H. Luo, L. Wang, Y. Huang, J. A. Rogers, *Proc. Natl. Acad. Sci. USA* **2015**, *112*, 11757.
- [21] B. J. M. Hausmann, B. J. Shields, Q. Quan, P. Maletinsky, M. McCutchenon, J. T. Choy, T. M. Babinec, A. Kubanek, A. Yacoby, M. D. Lukin, M. Lončar, *Nano Lett.* **2012**, *12*, 1578.
- [22] B. J. M. Hausmann, I. B. Bulu, P. B. Deotare, M. McCutcheon, M. L. Markham, D. J. Twitchen, M. Lončar, *Nano Lett.* **2013**, *13*, 1898.
- [23] B. J. M. Hausmann, B. J. Shields, Q. Quan, Y. Chu, N. P. de Leon, R. Evans, M. J. Burek, A. S. Zibrov, M. Markham, D. J. Twitchen, H. Park, M. D. Lukin, M. Lončar, *Nano Lett.* **2013**, *13*, 5791.
- [24] M. J. Burek, Y. Chu, M. S. Z. Liddy, P. Patel, J. Rochman, S. Meesala, W. Hong, Q. Quan, M. D. Lukin, M. Lončar, *Nat. Commun.* **2014**, *5*, 5718.
- [25] Y. Tao, J. M. Boss, B. A. Moores, C. L. Degen, *Nat. Commun.* **2014**, *5*, 3638.
- [26] V. P. Adiga, *Phys. Rev. B* **2009**, *79*, 245403.
- [27] T. H. Kim, W. M. Choi, D. H. Kim, M. A. Meitl, E. Menard, H. Jiang, J. A. Carlisle, A. Rogers, *Adv. Mater.* **2008**, *20*, 2171.
- [28] I. Aharonovich, A. D. Greentree, S. Prawer, *Nat. Photonics* **2011**, *5*, 397.
- [29] B. A. Fairchild, P. Olivero, S. Rubanov, A. D. Greentree, F. Waldermann, R. A. Taylor, I. Walmsley, J. M. Smith, S. Huntington, B. C. Gibson, D. N. Jamieson, S. Prawer, *Adv. Mater.* **2008**, *20*, 4793.
- [30] P. Olivero, S. Rubanov, P. Reichart, B. C. Gibson, S. T. Huntington, J. Rabeau, A. D. Greentree, J. Salzman, D. Moore, D. N. Jamieson, S. Prawer, *Adv. Mater.* **2005**, *17*, 2427.
- [31] T. Jung, L. Kreiner, C. Pauly, F. Mücklich, A. M. Edmonds, M. Markham, C. Becher, *Phys. Status Solidi A* **2016**, *10*, 1002.
- [32] S. D. Janssens, S. Drijkoningen, K. Haenen, *Appl. Phys. Lett.* **2014**, *104*, 073107.
- [33] L. A. Francis, A. Kromka, D. Steinmuller-Nethl, P. Bertrand, C. van Hoof, *IEEE Sens. J.* **2006**, *6*, 916.
- [34] A. P. Magyar, J. C. Lee, A. M. Limarga, I. Aharonovich, F. Rol, D. R. Clarke, M. Huang, E. L. Hu, *Appl. Phys. Lett.* **2011**, *99*, 81913.
- [35] M. J. Burek, N. P. Leon, B. J. Shields, B. J. M. Hausmann, Y. Chu, Q. Quan, A. S. Zibrov, H. Park, M. D. Lukin, M. Lončar, *Nano Lett.* **2012**, *12*, 6084.
- [36] T. M. Babinec, J. T. Choy, K. J. M. Smith, M. Khan, M. Lončar, *J. Vac. Sci. Technol. B* **2011**, *29*, 10601.
- [37] I. Bayn, B. Meyler, J. Salzman, R. Kalish, *New J. Phys.* **2011**, *13*, 25018.
- [38] V. Y. Prinz, V. A. Seleznev, A. K. Gutakovskiy, A. V. Chehovskiy, V. V. Preobrazhenskii, M. A. Putyato, T. A. Gavrilova, *Physica E* **2000**, *6*, 828.
- [39] E. J. Smith, W. Xi, D. Makarov, I. Mönch, S. Harazim, V. A. B. Quiñones, C. K. Schmidt, Y. Mei, S. Sanchez, O. G. Schmidt, *Lab Chip* **2012**, *12*, 1917.
- [40] W. Si, I. Mönch, C. Yan, J. Deng, S. Li, G. Lin, L. Han, Y. Mei, O. G. Schmidt, *Adv. Mater.* **2014**, *26*, 7973.
- [41] A. Bernardi, S. Kiravittaya, A. Rastelli, R. Songmuang, D. J. Thurmer, M. Benyoucef, O. G. Schmidt, *Appl. Phys. Lett.* **2008**, *93*, 094106.
- [42] Y. Mei, A. A. Solovev, S. Sanchez, O. G. Schmid, *Chem. Soc. Rev.* **2011**, *40*, 2109.
- [43] O. A. Williams, A. Kriele, J. Hees, M. Wolfer, W. Müller-Sebert, C. E. Nebel, *Chem. Phys. Lett.* **2010**, *495*, 84.
- [44] W. Huang, S. Koric, X. Yu, K. J. Hsia, X. Li, *Nano Lett.* **2014**, *14*, 6293.

- [45] O. Durand, J. Olivier, R. Bisaro, P. Galtier, J. K. Krüger, C. J. Brierley, G. R. Kennedy, *Appl. Phys. Lett.* **1999**, *75*, 1881.
- [46] Q. H. Fan, J. Gracio, E. Pereira, *J. Appl. Phys.* **2000**, *87*, 2880.
- [47] J. Timoshenko, *J. Opt. Soc. Am.* **1925**, *11*, 233.
- [48] R. Songmuang, C. Deneke, O. G. Schmidt, *Appl. Phys. Lett.* **2006**, *89*, 223109.
- [49] I. S. Chun, A. Challa, B. Derickson, K. J. Hisa, X. Li, *Nano Lett.* **2010**, *10*, 3927.
- [50] S. Alben, B. Balakrisnan, E. Smela, *Nano Lett.* **2011**, *11*, 2280.
- [51] Z. Chen, C. Majidi, D. J. Srolovitz, M. Haataja, *Appl. Phys. Lett.* **2011**, *98*, 011906.
- [52] S. Armon, E. Efrati, R. Kupferman, E. Sharon, *Science* **2011**, *333*, 1726.
- [53] Z. Chen, Q. Guo, C. Majidi, W. Chen, D. J. Srolovitz, M. P. Haataja, *Phys. Rev. Lett.* **2012**, *109*, 114302.
- [54] Q. Guo, A. K. Mehta, M. A. Grover, W. Chen, D. G. Lynn, Z. Chen, *Appl. Phys. Lett.* **2014**, *14*, 917.
- [55] M. Lončar, A. Faraon, *MRS Bull.* **2013**, *38*, 144.
- [56] Q. Guo, M. Zhang, Z. Xue, J. Zhang, G. Wang, D. Chen, Z. Mu, G. Huang, Y. Mei, Z. Di, X. Wang, *AIP Adv.* **2015**, *5*, 037115.
- [57] J. Wang, T. Zhan, G. Huang, P. K. Chu, Y. Mei, *Laser Photonics Rev.* **2014**, *8*, 521.
- [58] J. Philip, P. Hess, T. Feygelson, J. E. Butler, S. Chattopadhyay, K. H. Chen, L. Chen, *J. Appl. Phys.* **2003**, *93*, 2164.
- [59] J. Wang, T. Zhan, G. Huang, X. Cui, X. Hu, Y. Mei, *Opt. Express* **2012**, *20*, 18555.